ELSEVIER

Materials Science and Engineering B94 (2002) 247–259

MATERIALS SCIENCE & ENGINEERING B

www.elsevier.com/locate/mseb

An atomic-scale analysis of catalytically-assisted chemical vapor deposition of carbon nanotubes

M. Grujicic [a,*], G. Cao [a], Bonnie Gersten [b]

[a] *Department of Mechanical Engineering, Program in Materials Science and Engineering, Clemson University, Clemson, SC 29634, USA*
[b] *Army Research Laboratory—WMRD AMSRL-WM-MD, Aberdeen, Proving Ground, MD 21005-5069, USA*

Received 10 January 2002; accepted 4 March 2002

Abstract

Growth of carbon nanotubes during transition-metal particles catalytically-assisted thermal decomposition (also referred to as chemical vapor deposition or CVD) of methane in hydrogen as a carrier gas has been analyzed at the atomic scale using a kinetic Monte Carlo method. The method is parameterized by the rates of various nanotube surface and edge reactions (e.g. adsorption of hydrocarbons and hydrogen onto the surface of the transition-metal particles and onto the surface of carbon nanotubes, carbon atom attachment to the growing end of nanotubes, nucleation and growth of the outer nanotubes walls, etc.). Simulations of the carbon nanotubes growth are found to yield predictions regarding the effect of nominal and local processing conditions on the nanotubes morphology and growth rates in very good (qualitative and quantitative) agreement with their experimental counterparts. In addition, formation of new walls during growth is found to take place quite readily suggesting that the fabrication of single walled carbon nanotubes by CVD may be a formidable task.

Keywords: Carbon nanotubes; Chemical vapor deposition; Kinetic Monte Carlo method

1. Introduction

Since their discovery in 1991 [1], carbon nanotubes have attracted considerable interest because of their unique properties and potential applications such as: (a) their very high elastic modulus (600–650 GPa) in the direction of nanotubes axis makes them attractive as structural materials (e.g. [2]) and as probes in scanning probe microscopy [3]; (b) their high adsorption potential for hydrogen renders them promising materials for hydrogen storage devices (e.g. [4]); (c) their unique structure makes them suitable for tailored nanometer-scale membranes and molecular sieves [5]; (d) their high electrical conductivity renders them candidate materials for nanometer-scale wires [6], etc.

Carbon nanotubes are generally processed by laser ablation of carbon rods e.g. [7], a direct current arc-discharge between carbon electrodes in an inert-gas environment (e.g. [8]) or by transition-metal catalytically-assisted thermal decomposition of hydrocarbons (also refereed to as chemical vapor deposition or CVD) (e.g. [9]) in combination with nanofabricated catalytic patterning (e.g. [10]) and templating (e.g. [11]). The aim of these carbon nanotube fabrication processes is the production of long, uniform, single-walled carbon nanotubes, SWCNTs, since the properties of multi-walled carbon nanotubes, MWCNTs, are quite inferior compared to those of SWCNTs. In addition, it is generally desirable to process SWCNTs which are spatially ordered and of the same chirality. If the processing conditions are not selected properly, fabricated material typically consists of an amorphous-carbon infiltrated mat of poorly ordered entangled SWCNTs and MWCNTs with a wide distribution in nanotubes diameter and their structure varying between zigzag, armchair and other chiral forms.

Carbon nanotube modeling efforts can be roughly divided in two distinct categories: (a) molecular dynamics type calculations employing the Tersoff–Brenner reactive interatomic potentials (e.g. [12]) and (b) ab initio analyses based on density functional total energy

* Corresponding author. Address: 241 Engineering Innovation Building, Clemson University, Clemson, SC 29634-0921, USA. Tel.: +1-864-656-5639; fax: +1-864-656-4435.
E-mail address: mica.grujicic@ces.clemson.edu (M. Grujicic).

0921-5107/02/$ - see front matter
PII: S0921-5107(02)00095-8

Report Documentation Page

Form Approved
OMB No. 0704-0188

1. REPORT DATE	2. REPORT TYPE	3. DATES COVERED
2002		**00-00-2002 to 00-00-2002**

4. TITLE AND SUBTITLE	5a. CONTRACT NUMBER
An atomic-scale analysis of catalytically-assisted chemical vapor deposition of carbon nanotubes	5b. GRANT NUMBER
	5c. PROGRAM ELEMENT NUMBER
6. AUTHOR(S)	5d. PROJECT NUMBER
	5e. TASK NUMBER
	5f. WORK UNIT NUMBER
7. PERFORMING ORGANIZATION NAME(S) AND ADDRESS(ES) **Celmson University,Department of Mechanical Engineering,Clemson,SC,29634**	8. PERFORMING ORGANIZATION REPORT NUMBER
9. SPONSORING/MONITORING AGENCY NAME(S) AND ADDRESS(ES)	10. SPONSOR/MONITOR'S ACRONYM(S)
	11. SPONSOR/MONITOR'S REPORT NUMBER(S)

12. DISTRIBUTION/AVAILABILITY STATEMENT
Approved for public release; distribution unlimited

13. SUPPLEMENTARY NOTES

14. ABSTRACT

Growth of carbon nanotubes during transition-metal particles catalytically-assisted thermal decomposition (also referred to as chemical vapor deposition or CVD) of methane in hydrogen as a carrier gas has been analyzed at the atomic scale using a kinetic Monte Carlo method. The method is parameterized by the rates of various nanotube surface and edge reactions (e.g. adsorption of hydrocarbons and hydrogen onto the surface of the transition-metal particles and onto the surface of carbon nanotubes, carbon atom attachment to the growing end of nanotubes, nucleation and growth of the outer nanotubes walls, etc.). Simulations of the carbon nanotubes growth are found to yield predictions regarding the effect of nominal and local processing conditions on the nanotubes morphology and growth rates in very good (qualitative and quantitative) agreement with their experimental counterparts. In addition, formation of new walls during growth is found to take place quite readily suggesting that the fabrication of single walled carbon nanotubes by CVD may be a formidable task.

15. SUBJECT TERMS

16. SECURITY CLASSIFICATION OF:			17. LIMITATION OF ABSTRACT	18. NUMBER OF PAGES	19a. NAME OF RESPONSIBLE PERSON
a. REPORT **unclassified**	b. ABSTRACT **unclassified**	c. THIS PAGE **unclassified**	**Same as Report (SAR)**	**13**	

calculations (e.g. [13]) often combined with molecular dynamics simulations (e.g. [14]). These modeling approaches enable elucidation of the basic mechanisms and the underlying energetic associated with the growth of SWCNTs and MWCNTs in the absence and in the presence of transition-metal catalysts. However, these methods are not very useful in helping establish relationships between the fabrication–process parameters (e.g. temperature, pressure, gas-phase chemistry, etc.) and the nucleation and growth conditions at the surface/edges of growing nanotubes, the conditions which control nanostructure, length and spatial ordering, and thus properties of nanotubes. In a series of papers, Grujicic and Lai [15–17] demonstrated that establishment of the process-parameters/growth-conditions/materials microstructure relationships entails a multi length-scale approach. That is, the same problem, (fabrication of the carbon nanotubes, in the present case) must be considered at the length scale of a chemical reactor, at the characteristic length-scale of a growing nanotube and at the atomic length scale. Recently, Grujicic et al. [18,19] developed a reactor-length scale model for carbon nanotubes fabrication via transition-metal particles catalytically-assisted thermal decomposition of methane. The results of the reactor-scale model developed by Grujicic et al. [18,19] (specifically the concentrations of gas-phase species at the surface and edges of nanotubes and the rate of attachment of carbon atoms to the growing end of carbon nanotubes) are used as a boundary condition in the present work to carry out atomic-scale simulations of the growth and microstructure evolution of carbon nanotubes during the fabrication process via transition-metal particles catalytically-assisted thermal decomposition of methane.

Due to the use of lower temperatures, higher controllability of the process and generally higher yields, transition-metal particles assisted CVD appears to be a very attractive route for fabrication of carbon nanotubes. However, carbon nanotubes processed via thermal decomposition of hydrocarbons are generally MWCNTs and, hence, have inferior properties relative to their SWCNT counterparts. Therefore, the main objective of the present work is to help understand the basic mechanism for formation of MWCNTs, and, if possible, identify CVD processing conditions which promote formation of SWCNTs.

The organization of the paper is as follows. A brief overview of the procedure used to construct the rigid-lattice framework is presented in Section 2.1. Nanotubes surface and edge reaction mechanisms accompanying thermal decomposition of a CH_4+H_2 gas mixture and the underlying reaction kinetics are discussed in Section 2.2. The kinetic Monte Carlo method used for atomic length-scale simulation of carbon nanotubes growth and nanostructure evolution is briefly reviewed in Section 2.3. The results obtained in the present work are presented and discussed in Section 3. The main conclusion resulted from the present work are summarized in Section 4.

2. Computational procedure

2.1. Generation of multi-wall carbon nanotube lattice

Scanning and transmission electron microscopy investigations of SWCNTs and MWCNTs fabricated using either of the three aforementioned methods (catalytically-assisted by fine transition-metal particles) reveal two distinct mechanisms of nanotubes growth: (a) the so called 'root-growth' mechanism [23] in which the catalytic particle remains on the substrate (reactor wall) and thus in the root of the nanotube as the nanotube grows in a direction normal to the reactor wall, Fig. 1(a); and (b) the so called 'tip-growth' mechanism [23] in which the catalytic particle detaches from the substrate and moves to the tip of the growing nanotubes, Fig. 1(b). Since carbon nanotubes processed via transition-metal particles catalytically-assisted thermal decomposition of hydrocarbons are generally found to grow via the tip-growth mechanism e.g. [9], only this growth mechanism is considered in the present work. Moreover, the nucleation of the innermost wall of MWCNTs is not analyzed. Rather, it is assumed that a short SWCNT whose diameter is equal to that of the innermost wall of MWCNT with a transition-metal particle attached to its tip is present from the onset of computer simulations.

The growth of carbon nanotubes has been simulated using a rigid-lattice approach within which atomic relaxations and vibrations are not considered. Rather atoms are assumed to reside on fixed lattice sites. Since atomic scale simulations are very computer intensive, only growth of four-wall carbon nanotubes has been

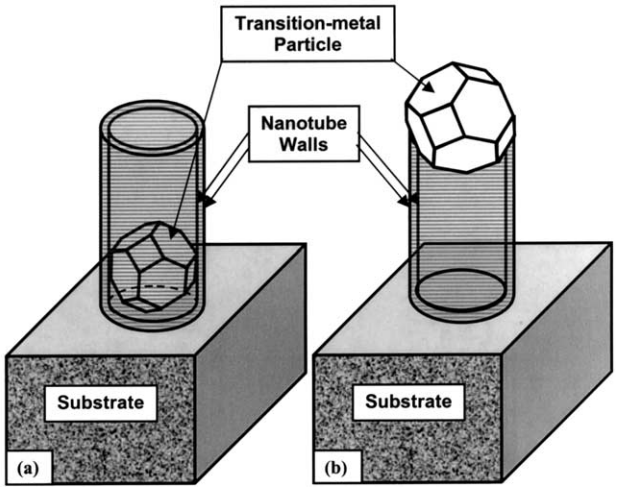

Fig. 1. A schematic of (a) the root-growth mechanism; and (b) the tip-growth mechanism of carbon nanotubes growth.

carried out in the present work. Toward that end, eight rigid lattices are used: (a) a $(n, m) = (10, 10)$ armchair type lattice with a radius of 0.675 nm which is used for simulation of the growth of the innermost wall of a four-wall carbon nanotube, Fig. 2(a). The vector (n, m) indicates the direction in which a one-atom thick strip of graphite of a (n, m)-dependent width should be rolled up in order to produce a given nanotube (n and m are the components of the roll-up vector in $[\bar{1}\ 1\ 0\ 0]$ and $[\bar{1}\ 0\ 1\ 0]$ directions, respectively). MWCNTs based on (10, 10) armchair type nanotubes are generally observed in CVD processed carbon nanotubes e.g. [9] and that is the reason for selection of the (10, 10) armchair nanotube in the present work; (b) a triagonal cylindrical lattice with a radius of 1.013 nm, Fig. 1(b), which is used to model the adsorption of hydrocarbons and hydrogen atoms from the gas phase onto the (10, 10) innermost wall; (c) a (15, 15) armchair type lattice with a radius of 1.013 nm used for simulation of the growth of the second wall of the four-wall carbon nanotube, Fig. 2(c); (d) a triagonal cylindrical lattice with a radius of 1.351 nm, Fig. 2(d), used to model the adsorption of hydrocarbon and hydrogen atoms from the gas-phase; (e) a (20, 20) armchair type lattice with a radius 1.351 nm (not shown for brevity) used for simulation of the growth of the third nanotube wall; (f) a triagonal cylindrical lattice with a radius of 1.689 nm (not shown for brevity) used for modeling of the adsorption of gas-phase species on the third nanotube wall; (g) a (25, 25) armchair type lattice with a radius 1.689 nm (not shown for brevity) used for modeling of the growth of forth (outermost) wall of the nanotube; and (g) a triagonal cylindrical lattice with a radius of 2.026 nm (not shown for brevity) used for simulation of the gas-phase species adsorption to the outermost wall. It should be noted that in order to improve clarity, only short segments of the first four lattices are displayed in Fig. 2(a)–(d).

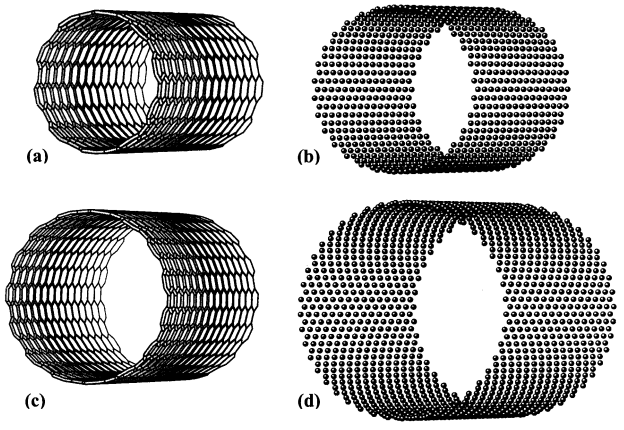

Fig. 2. (a) (10, 10) carbon nanotube; (b) innermost triagonal; (c) (15, 15) carbon nanotube; and (d) second triagonal rigid lattices used in the present atomic-scale analysis of growth and nanostructure evolution. Small spheres in (b) and (d) denote lattice sites.

Furthermore, to better utilize the space available for the figure, the nanotube axis is selected to be horizontal in Fig. 2(a)–(d). Typically, horizontal-type cylindrical CVD reactors are used for nanotube fabrication so the nanotubes grow in a direction orthogonal to the reactor wall.

At the beginning of a simulation run, it is assumed that a short (length ≈ 0.48 nm) (10, 10) armchair nanotube has nucleated on the lattice displayed in Fig. 2(a) and that its root is attached to a substrate (e.g. the wall of the CVD reactor) while its tip (the growing end) is 'capped' with a transition-metal particle, Fig. 1(b). The presence of the transition-metal particle is considered only indirectly. That is, its effect in promoting adsorption of hydrocarbons and attachment of carbon atoms to the growing end of the carbon nanotube is considered, while no lattice is used to represent the surface (or volume) of the particle. Also, the nanotube is assumed to grow only at the end which is in contact with the transition metal particle. The other end of the carbon nanotube, as discussed earlier, is assumed to be attached to the reactor wall and remains stationary during the simulation process.

As simulation proceeds, adsorption of hydrocarbons and hydrogen onto the innermost triagonal lattice shown in Fig. 2(b) takes place. As will be discussed in more details in Section 2.2, hydrogen abstraction from the adsorbed hydrocarbon molecules which results in formation of (adsorbed) mobile carbon atoms can give rise to nucleation (and subsequent growth) of the second (15, 15) wall of the nanotube, on the lattice shown in Fig. 2(c).

Once the second wall of the nanotube has nucleated, hydrocarbons and hydrogen are allowed to adsorb to its surface/edge i.e. onto the triagonal lattice depicted in Fig. 2(d). Hydrogen abstraction from the triagonal lattice shown in Fig. 2(d) is then allowed to take place which can ultimately lead to nucleation (and subsequent growth) of the third (20, 20) nanotube wall. In the same way adsorption of gas-phase species and hydrogen abstraction on the third nanotube wall, and the resulting nucleation of the forth (25, 25) nanotube wall are modeled.

The adsorption lattice shown in Fig. 2(b) is chosen to be simple triagonal and, thus, to contain the same number of hexagons as the inner (10, 10) carbon nanotube lattice. However, since the radius of the adsorption lattice (1.002 nm) is larger than that of the inner nanotube wall (0.668 nm), hexagons in the former lattice are proportionally larger relative to those in the latter. Also, the adsorption lattice contains additional site, the site located at the center of hexagons, and thus enables species adsorptions on both the bridge sites (the sites halfway between the two adjacent carbon atoms in the graphite structure) and the center sites (the site coinciding with the hexagons centers). These sites have

been identified by Lee et al. [13] using density functional total energy calculations as primary carbon-nanotubes adsorption sites. It should be noted that, since the innermost adsorption lattice contains 50% more lattice sites relative to the graphite type lattice of carbon nanotubes, its number of lattice sites is identical to that of the (15, 15) carbon nanotube lattice (the second nanotube wall). When the second wall is nucleated (or continues to grow), carbon atoms forming the second wall are transferred from the innermost triagonal adsorption lattice shown in Fig. 2(b) to the (15, 15) carbon nanotube lattice. To enable such transfer, a one-to-one correspondence is established between the sites of two lattices. Once an atom has been transferred from the adsorption lattice to the (15, 15) nanotube lattice, the site on the former lattice from which the atom is transferred is removed and not any longer allowed to contain a species.

The (second) adsorption lattice shown in Fig. 2(d) is also chosen to be simple triagonal and to contain the same number of hexagons as the (15, 15) carbon nanotube lattice. However, in order to achieve a one-to-one correspondence between the sites of the second adsorption lattice and the ones of the (20, 20) nanotube lattice, randomly selected sites on the adsorption lattice which correspond to hexagons centers are excluded from the gas-phase species adsorption process and thus from the nanotube wall nucleation process. Similar procedures are followed while constructing the remaining (outermost) two adsorption lattices.

2.2. Nanotube surface and edge reaction mechanisms and kinetics

In this section, a brief overview is given of the basic mechanisms and the underlying kinetics accompanying growth of carbon nanotubes. As stated in the previous section, a short (10, 10) armchair type nanotube is assumed to exist from the onset of simulation. The root of this nanotube is assumed to be stationary and attached to the reactor wall. A small transition-metal particle is assumed to adhere to tip of the nanotube. While the particle is not considered explicitly in the present work, its effect on the carbon nanotube growth is incorporated by including the rates at which carbon atoms diffusing over the particle surface attach to be growing end of the nanotube or are transferred to the nanotube surface. Values for these rates for a wide range of processing conditions associated with co-particles assisted thermal decomposition of methane have been obtained in our recent work dealing with reactor-length scale modeling of the carbon nanotubes fabrication process [18,19]. In that work, carbon nanotubes fabrication by catalytically-assisted thermal decomposition of methane in a CH_4+H_2 gas mixture has been studied by solving a continuum coupled boundary-layer laminar-flow hydrodynamics, heat transfer, gas-phase chemistry and surface chemistry problem. The solution of such problem yields the concentrations of gas-phase species at the nanotube surface and the rates of carbon attachment to the tip of nanotubes, the quantities which serve as direct input (i.e. boundary conditions) to the present atomic-scale analysis of nanotube growth and nanostructure evolution.

Atomic-scale modeling of carbon nanotubes growth has been carried out using a kinetic approach within which all processes taking place at the surface and the tip of nanotubes have been considered as surface or edge reactions. The kinetics of such reactions is represented using the general formalism as used in the SURFACE CHEMKIN computer program and thermochemical database [20]. Within this formalism, the forward rate constant for reaction i, k_{fi}, is assumed to be defined by the following Arrhenius-type relation:

$$k_{fi} = A_i T^{\beta_i} \exp\left(-\frac{E_i}{RT}\right) \tag{1}$$

where the pre-exponential factor A_i, the temperature exponent β_i and the activation energy E_i, for all the surface/edge reactions considered in the present work are listed in Table 1, R is the universal gas constant and T is the absolute temperature.

For reversible reactions, the reverse reaction rate constant is related to the forward reaction rate constant via the following equation:

$$k_{ri} = \frac{k_{fi}}{K_{Ci}} \tag{2}$$

where K_{Ci} is the equilibrium reaction constant expressed in concentration units and is related to the equilibrium reaction constant expressed in pressure units, K_{Pi} as:

$$K_{Pi} = K_{Ci}\left(\frac{P_{atm}}{RT}\right)^{-\sum_{k=1}^{K_g} v_{ki}} \prod_{n=1}^{N_n} (\Gamma_n^0)^{-\sum_{k=1}^{K(n)} v_{ki}} \times \prod_{k=1}^{K(n)} \sigma_k^{v_{ki}} \tag{3}$$

where P_{atm} is the pressure of 1 atm, N_n, the number of types of surface sites, $\Gamma_n{}^0$ standard state density of the surface sites of type n, $\sigma_k(n)$ the number of sites of type n occupied by species k, and v_{ki}s are the stoichiometric reaction coefficients associated with species k and reaction i, K_g the total number of gas-phase species and $K(n)$ the number of species residing on the sites of type n. All nanotubes surface lattice sites and all edge sites are considered to be identical in the present work and hence n is set to unity.

The equilibrium reaction constant K_{Pi} can be computed from the standard-state enthalpy change $\Delta H_i{}^0$ and the standard state entropy change $\Delta S_i{}^0$ accompanying reaction i as:

Table 1
Nanotube surface and end reactions accompanying nanotube growth and the corresponding kinetic parameters

No.	Reaction	A [a]	β [a]	E [a]	ΔH^{0a}	ΔS^{0a}
Adsorption/desorption reactions						
R1	$S+H(G)\leftrightarrow H(S)$	8.6×10^{12}	0.0	0.0	–[b]	–[b]
R2	$S+CH_3(G)\leftrightarrow CH_3(S)$	4.9×10^{11}	0.0	0.0	–[b]	–[b]
Hydrogen-abstraction reactions						
R3	$H(S)+H(G)\leftrightarrow H_2(G)$	1.1×10^{12}	0.0	7300.0	–[b]	–[b]
R4	$CH_3(S)+H(G)\leftrightarrow CH_2(S,R)+H_2(G)$	2.8×10^{7}	2.0	7700.0	−11 300	6.6
R5	$CH_2(S,R)+H(G)\leftrightarrow CH(S,R_2)+H_2(G)$	2.8×10^{7}	2.0	7700.0	−11 300	6.6
R6	$CH(S,R_2)+H(G)\leftrightarrow C(S,R_3)+H_2(G)$	2.8×10^{7}	2.0	7700.0	−11 300	6.6
Radical-recombination reactions						
R7	$CH_2(S,R)+H(G)\leftrightarrow CH_3(S)$	5.0×10^{12}	0.0	0.0	−70 900	−42.0
R8	$CH(S,R_2)+H(G)\leftrightarrow CH_2(S,R)$	5.0×10^{12}	0.0	0.0	−70 900	−42.0
R9	$C(S,R_3)+H(G)\leftrightarrow CH(S,R_2)$	5.0×10^{12}	0.0	0.0	−70 900	−42.0
Nanotube-surface diffusion of hydrogen and carbon						
R10	$H(S_1)+S_2\leftrightarrow s_1+H(S_2)$	1.3×10^{12}	0.0	33 060.0	0.0	0.0
R11	$C(s_1)+S_2\leftrightarrow S_1+C(S_2)$	1.3×10^{12}	0.0	33 898.0	0.0	0.0
Nucleation of the outer nanotube wall						
R12	$nC(S)\leftrightarrow nC(NT)$ $(n\geq4)$	1.3×10^{12}	0.0	35 743.0	–[c]	–[c]
Growth of the outer nanotube wall						
R13	$C(S)+nC(NT)\leftrightarrow(n+1)C(NT)$	1.3×10^{12}	0.0	30 785.0	–[c]	–[c]
Carbon attachment to the edge of the inner wall						
R14	$C(S)+E\leftrightarrow S+C(E)$	1.3×10^{12}	0.0	31 104.0	–[c]	–[c]
R15	$C(S_{TM})+E\leftrightarrow S_{TM}+C(E)$	1.3×10^{12}	0.0	31 104.0	–[c]	–[c]
Nanotube-edge diffusion of carbon						
R16	$C(E_1)+E_2\leftrightarrow E_1+C(E_2)$	1.8×10^{11}	0.0	47 734.0	0.0	0.0
Transition-metal particle induced carbon atom transfer onto the nanotube surface						
R17	$C(S_{TM})+S\leftrightarrow S_{TM}+C(S)$	1.3×10^{12}	0.0	31 104.0	–[c]	–[c]

[a] The unit for A is given in terms of moles, cubic centimeters and seconds and for E as cal mole^{-1}. β is unitless.
[b] The parameter is calculated at a given temperature using the six-term series expansions as defined in the SURFACE CHEMKIN thermochemical database [20].
[c] The parameter is not needed in the present calculation.

$$K_{Pi}=\exp\left(\frac{\Delta S_i^0}{R}-\frac{\Delta H_i^0}{RT}\right) \tag{4}$$

Values for $\Delta H_i{}^0$ and $\Delta S_i{}^0$ for the set of nanotubes surface/edge reactions used in the present work are listed in Table 1. It should be noted that for the reactions which do not change the number of species (e.g. reactions R4, R5, R6, etc. in Table 1), $\Sigma_{k=1}^{K_g}\nu_{ki}=0$, and hence $(P_{atm}/RT)^{\Sigma_{k=1}^{K_g}\nu_{ki}}=1$, which greatly simplifies Eq. (3). For the reactions for which the number of species is reduced by one (e.g. reactions R1, R2 and R3, Table 1), $\Sigma_{k=1}^{K_g}\nu_{ki}=-1$, and hence $(P_{atm}/RT)^{\Sigma_{k=1}^{K_g}\nu_{ki}}=0.0122\ \ \mathrm{K\ cm^{-3}}\times(1/T(\mathrm{K}))$.

As indicated in Table 1, a number of nanotube surface and edge reactions accompanies growth of carbon nanotubes during transition-metal particles assisted thermal decomposition of methane. These reactions can be generally classified as:

2.2.1. Surface adsorption reactions: (R1, R2)

Hydrogen and hydrocarbon molecules from the gas phase are adsorbed on to the surface of a nanotube (more precisely onto the simple triagonal adsorption lattices). As demonstrated in our previous work [18,19], CH_3 is the main hydrocarbon species present during carbon nanotube growth via thermal decomposition of methane. Hence, only adsorption of CH_3 and atomic hydrogen (H) has been considered in the present work, Table 1. It should be noted that the following nomenclature is used in Table 1: S—a surface site on the adsorption lattice; (G)—a gas-phase species; (S)—a surface species; (R), (R_2) and (R_3)—single, double and triple radical species; S1 and S2—two adjacent surface sites; S_{TM}—a site on the surface of a transition-metal particle; E—an edge site at the tip of a nanotube; and C(NT)—a carbon atom on the non-innermost wall of a nanotube.

The Arrhenius kinetic parameters for CH_3 and H adsorption onto the surface of nanotubes listed in Table

1 have been determined in our recent work [19]. The standard-state enthalpy ΔH^0 and the standard state entropy ΔS^0 changes which control the reverse (desorption) reaction rates of CH_3 and H have been obtained at a given temperature using the appropriate six-term temperature expansion series as defined in the SURFACE CHEMKIN thermochemical database [20].

2.2.2. Hydrogen abstraction reaction: (R3–R6)

Atomic hydrogen adsorbed at the surface of carbon nanotubes can be adsorbed via a reaction with the atomic gas-phase hydrogen (reaction R3). Furthermore, hydrocarbon molecules adsorbed on the nanotube surface can undergo a series of hydrogen abstraction reactions (R4–R6) whose ultimate result is formation of the (absorbed) carbon atoms. The Arrhenius kinetic parameters for hydrogen abstraction for adsorbed atomic hydrogen are taken from our recent work [19] while those for the hydrogen abstraction from adsorbed CH_3 were reported by Grujicic and Lai [15]. The standard-state enthalpy ΔH^0 and the standard state entropy ΔS^0 changes associated with the reverse hydrogen-abstraction reaction of adsorbed atomic hydrogen at a given temperature are obtained using the appropriate six-term temperature expansion series discussed above [20]. The same quantities but for hydrogen abstraction from $CH_3(S)$, $CH_2(S,R)$, $CH(S,R_2)$ are obtained from Grujicic and Lai [15].

2.2.3. Radical recombination reaction: (R7–R9)

Hydrocarbon radicals formed during hydrogen abstraction reactions can react with atomic gas-phase hydrogen to eliminate one or more dangling bonds. The Arrhenius kinetic parameters for such radical recombination reactions are taken from Grujicic and Lai [15]. The standardstate enthalpy ΔH^0 and the standard state entropy ΔS^0 changes which are used for the calculation of the corresponding reverse (radical recombination) reactions are also obtained from Grujicic and Lai [15].

2.2.4. Surface diffusion reaction: (R10, R11)

Adsorbed hydrogen and carbon, due to their relatively small atomic size are assumed to diffuse over the surface of the carbon nanotubes. On the other hand, CH_3 and the hydrocarbon radicals produced during hydrogen abstraction from CH_3 are assumed to be immobile due to a relatively large size of their molecules. The activation energy term, E, for surface diffusion of carbon and hydrogen are obtained using the density functional total energy calculation results of Lee et al. [21]. The pre-exponential kinetic parameter A is calculated using density functional total energy calculation results of Kitamura and Oshiyama [24] and a simple linear-oscillator approximation as:

$$A = \frac{1}{2}\sqrt{\frac{b}{m}} \tag{5}$$

where b is the second derivative of the total energy in the direction of atomic jump evaluated at the minimum energy position of the diffusing atom and m is the mass of the same atom. Furthermore, the rates of forward and reverse reactions are considered to be equal which is attained by setting both ΔH^0 and ΔS^0 to zero.

2.2.5. Nucleation of the non-innermost walls: (R12)

When the number of adsorbed nearest-neighbor carbon atoms reaches (or exceeds) a critical value, they can rearrange themselves into a graphite-like structure to nucleate the outer wall of the nanotube. By carrying out a series of Tersoff–Brenner potential based molecular statics calculations of the potential energy of various surface clusters of carbon atoms [28], the critical number of carbon atoms required for nucleation is assessed as 10 and is assumed to be independent of the CVD processing conditions. The activation energy term, E, for nucleation of the outer wall of a carbon nanotube is computed using the density functional total energy calculation results of Lee et al. [21]. This was done by subtracting an average energy of the ten adjacent adsorbed carbon atoms from that for the ten corresponding atoms in the newly-nucleated wall of the nanotube. The pre-exponential term A is set equal to that for surface diffusion of the carbon atoms. The nucleation reaction is assumed to be irreversible which eliminates the need for specifying the values for ΔH^0 and ΔS^0.

2.2.6. Growth of the non-innermost walls: (R13)

When an adsorbed carbon atom is adjacent to a nucleus of a (non-innermost) wall of a nanotube, it can attach to the nucleus giving rise to its growth. An average value of the activation energy for growth of the outer wall of a carbon nanotube is obtained using the data obtained in the work of Lee et al. [21]. This was done, by subtracting the average energy of an adsorbed carbon atom from that for a carbon atom at the edge of a nucleus of the newly nucleated wall of a nanotube. The pre-exponential term A is again set equal to that for surface diffusion of the carbon atoms. The growth process of a (non-innermost) wall is also considered to be irreversible, so that ΔH^0 and ΔS^0 values did not need to be defined.

2.2.7. Carbon attachment to the nanotube tip: (R14, R15)

The inner nanotube growth is considered to take place as a result of attachment of carbon atoms to the growing end of nanotubes walls. Carbon atoms which can attach themselves to the tip of the walls are either those which

are adsorbed onto and diffuse over the corresponding adsorption lattice (reaction R14) or those adsorbed onto and diffusing over the surface of the transition-metal particle (reaction R15). Both reactions R14 and R15 are assumed to be irreversible eliminating the need for knowledge of the ΔH^0 and ΔS^0 values. The kinetic parameters A, β and E for both reactions are obtained by fitting the corresponding computed nanotube growth data obtained in our recent work [18] to the Arrhenius functional form, Eq. (1). An example of this procedure for the rate of carbon atom attachment to the nanotube tip is shown in Fig. 3 in which the logarithm of the reaction rate is plotted again the inverse temperature. The discrete points denote the results obtained in our previous work [18], while the solid line shows the fitting curve obtained using a non-linear least-square procedure based on the Genetic Algorithm [25].

2.2.8. Diffusion of carbon along the nanotube edge: (R16)

Carbon atoms attached to the tip of a carbon nanotube are allowed to diffuse over the nanotube edge. Activation energy, E, and the pre-exponential term, A, for carbon diffusion along carbon nanotube edge are obtained using the aforementioned procedure applied to the surface diffusion and the results of Kitamura and Oshiyama [24] who carried out density functional total energy calculation of carbon nanotube growth. The forward and reverse diffusion rate are taken to be equal by setting $\Delta H^0 = 0$ and $\Delta S^0 = 0$.

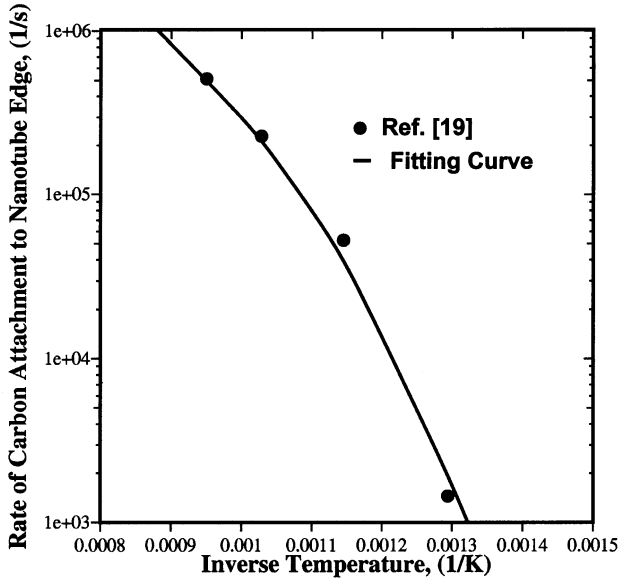

Fig. 3. Temperature dependence of the rate of carbon-atom attachment to the nanotube edge.

2.2.9. Transfer of carbon atoms diffusing over the surface of the transition-metal particle to the nanotubes surface: (R17)

Carbon diffusing over the surface of the transition metal particle can not only get attached to the nanotube edge but also can jump to one of the surface sites of the outermost wall of the nanotube in the vicinity of the nanotube edge. If the local concentration of such carbon atoms becomes large enough, it can lead to the nucleation of a new wall of the nanotube. Due to a large difference in the energies of a carbon atom at the surface of a transition-metal particle and that at the surface of a carbon nanotube [19], reaction R17 is assumed to be irreversible and hence, ΔH^0 and ΔS^0 values are not needed. The activation energy E for this reaction is obtained in our previous work [19], while the pre-exponential term A is set equal to that for surface diffusion of carbon.

2.3. Kinetic Monte Carlo method

The temporal evolution of the nanotubes morphology during nanotubes growth is simulated using the kinetic Monte Carlo method recently developed by Battaile et al. [22]. Within this method, one surface/edge reaction is allowed to take place at one nanotube surface/edge site during each time step. The occurrence of one of the reactions at one of the sites is termed an event. At each time step, a list of all possible events is constructed and the probability for each event is set proportional to the rate of the associated surface reaction scaled by a sum of the rates of all possible events. Next, a random number α uniformly distributed in the range (0, 1) is generated and used to select an event m from M possible events in accordance with the relation:

$$\sum_{j=0}^{m-1} r_j \Big/ \sum_{j=0}^{M} r_j < \alpha < \sum_{j=0}^{m} r_j \Big/ \sum_{j=0}^{M} r_j \tag{6}$$

where r_j is the rate of surface reaction associated with event j, and $r_0 = 0$.

When a surface/edge chemical reaction involves a gas-phase reactant k (e.g. H(G) in reaction Rl), the rate of the reaction is calculated under the assumption that mass-action kinetics is obeyed. That is, the reaction rate is defined as the product of the reaction rate constant and the molar concentration of the gas-phase reactant at the nanotube surface/edge raised to a power which is equal to its stoichiometric coefficient in the chemical reaction at hand. The concentration (site fraction) of the surface species involved in the same reaction at a given lattice site is set, however, to 1.0. That is, if a reaction is feasible at a given lattice site, the reacting surface species must be present at that site. Otherwise, if the species is not present (its site fraction is equal to zero) at a given lattice site, the reaction in question is not feasible.

Following the same approach, the rates of surface/edge reactions which involve only surface/edge species is set equal to the corresponding reaction rate constant. For all surface/edge reactions, however the reaction rate has units of $(\text{time})^{-1}$.

After an event has occurred, the total number of possible events M, and the sequence in which the events are listed in the event table are updated and the aforementioned procedure for random selection of an event is repeated for the next time step.

The kinetic Monte Carlo method used in the present work uses a variable time step to account for the fact that different events take place at different rates. At each simulation step, the time increment Δt is computed as:

$$\Delta t = -\ln(\beta) \Big/ \sum_{i=1}^{M} r_i \tag{7}$$

where β is a random number uniformly distributed in the range (0, 1), and the denomination in Eq. (7) represents the sum of the reaction rates of all the events that can occur at the given simulation step. The time increment given by Eq. (7) is hence adjusted dynamically and stochastically to accommodate the fastest possible event at each simulation step, greatly reducing restrictions associated with the conventional fixed time-increment methods. In other words, when fast events are possible in a given step, the denominator in Eq. (7) is large and, thus, Δt is small (i.e. the time scale is fine). Conversely, when only slow events are possible during a simulation step, the time increment is large (i.e. the time scale is coarse). The expression for the time increment given in Eq. (7) is rigorous and its derivation is presented in Appendix A.

3. Results and discussion

The atomic-scale kinetic Monte Carlo method overviewed in Section 2.3 is employed in this section to analyze carbon nanotubes growth from a H_2+18 mol% CH_4 mixture in the presence of cobalt catalytic particles for two different sets of nominal CVD processing parameters. The first set of these parameters (pressure = 1 atm, the axial flow rate of the gas mixture at the reactor inlet = 90 cm min^{-1}, the gas mixture temperature at the reactor inlet = 573 K, and the reactor-wall temperature = 1023 K) correspond to the one used in the experimental work of Buckenstein and Hu [26]. It should be noted that, as shown in our previous work [8], for the given set of nominal CVD processing parameters, the local processing conditions (e.g. temperature of the gas mixture, chemical composition of the gas mixture, etc.) can vary considerably along the length of the reactor. To determine the effect of variations in the local processing conditions on the growth and morphology of nanotubes, atomic scale simulations are carried out in the present work using local processing conditions (gas temperature, concentration of gas-phase species rate of carbon atom attachment to the nanotubes tip) at the following three axial locations of a 1-foot long horizontal CVD reactor: (a) the location which is 1 in. away from the reactor entrance; (b) the reactor midpoint; and (c) the location which is 1 in. away from the reactor exit.

The second set of CVD processing parameters correspond to the one used in the experimental work of Flahaut et al. [27]. The only significant difference between these processing conditions and the ones used by Buckenstein and Hu [26] is a substantially higher reactor-wall temperature (1343 vs. 1023 K) used in the work of Flahaut et al. [27]. Again, to examine the effect of reactions of the local CVD processing conditions on the growth and morphology of nanotubes, the local processing conditions associated with the same three axial locations as discussed above, are used.

Evolution of the carbon nanotube morphology during growth under the CVD processing conditions corresponding to those used by Buckenstein and Hu [26] as a function of the simulation time at the midpoint of the chemical reactor is displayed in Fig. 4(a)–(c). It should be noted that in each of these figure, the nanotube grows in a near two o'clock direction. At the shortest time displayed (~ 1 s), Fig. 4(a), the initial (10, 10) SWCNT has grown from its starting length of 0.48 nm to a length of approximately 25 nm. In addition, the second (15, 15) nanotube wall has nucleated near the growing end of the nanotube (the end which is contact with the transition metal particle). The tips of both nanotube walls are rough indicating the stochastic nature of the growth process and relatively sluggish edge diffusion.

At the simulation time of ~ 3.2 s, Fig. 4(b), the innermost (10, 10) and the second (15, 15) nanotube walls have grown to a length of approximately 44 nm and the third (20, 20) nanotube wall has nucleated (again next to the growing end of the nanotube). In addition to growing in the forward direction, the second (15, 15) nanotube wall has also grown in the reverse direction and, at the time of nucleation of the third (20, 20) nanotube wall, the second (15, 15) nanotube wall has grown all the way to the other (stationary) end of the nanotube. It should be noted that only the portion of the nanotube next to its growing end is shown in Fig. 4(b) in order to achieve clarity of the nanotube morphology displayed in this figure.

After 6.5 s of the simulation time, Fig. 4(c), the innermost (10, 10), the second (15, 15) and the third (20, 20) nanotube walls have grown to a length of approximately 60 nm and the fourth (25, 25) nanotube wall has nucleated (once more in the vicinity of the growing end of the nanotube). In addition, by this time the third (20, 20) nanotube wall has extended in the reverse direction

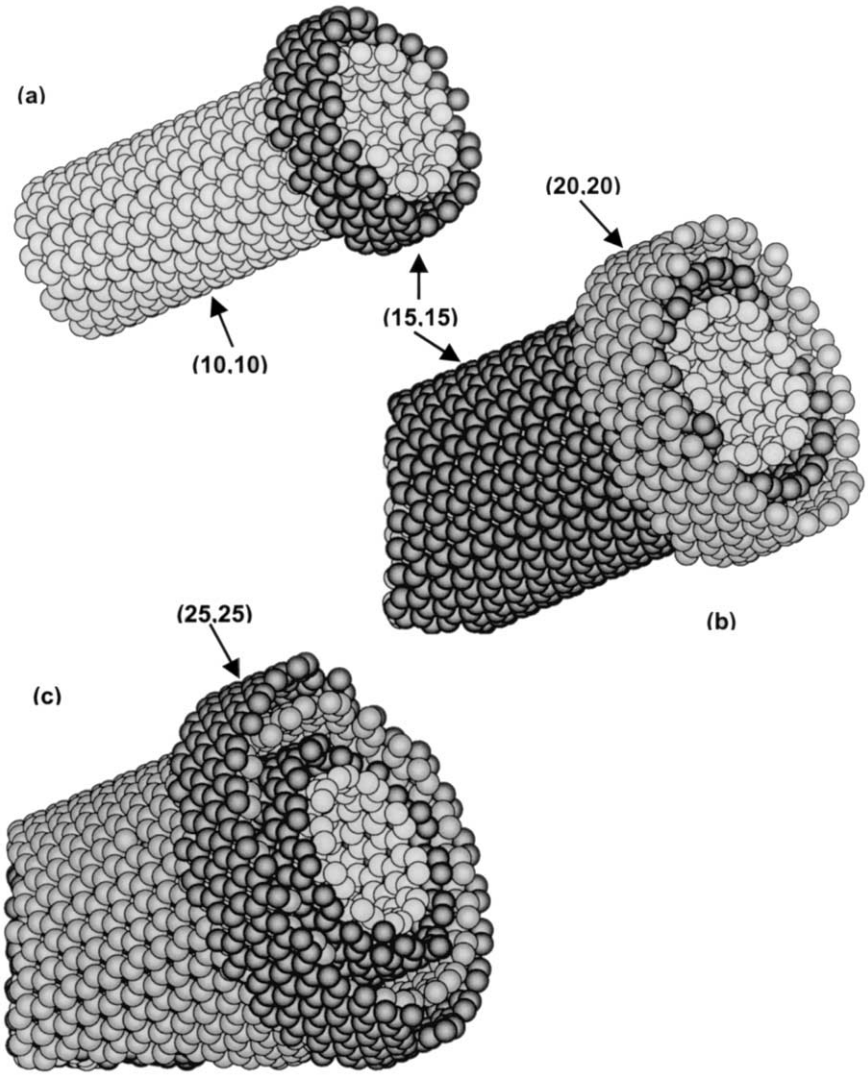

Fig. 4. The nanotube morphology at three different simulation times: (a) l s; (b) 3.2 s; and (c) 6.5 s. The corresponding total nanotube lengths are ~25, ~44 and ~60 nm, respectively. The CVD processing conditions correspond to the ones used by Buckenstein and Hu [26].

all the way to the stationary end of the nanotube (again, the entire nanotube is not shown in Fig. 4(c) for clarity).

Temporal evolution of the lengths of the four nanotube walls during growth under the CVD processing conditions consistent with the ones used by Buckenstein and Hu [26] at the axial location corresponding to the midpoint of the reactor are displayed in Fig. 5(a). At the beginning of the simulation process, only the (10, 10) wall is present and, consequently, its growth rate is quite high (around 23 nm s^{-1}). After the second (15, 15) nanotube wall has nucleated at the simulation time of ~1 s, the growth rate of the (10, 10) nanotube wall decreases to about 9 nm s^{-1}. This nearly 60% decrease in the growth rate is consistent with the associated increase in the average number of the edge sites (20 in a (10, 10) SWCNT vs. 50 in a (10, 10)+(15, 15) two-wall carbon nanotube). The results shown in Fig. 5(a) also indicate that, after the second (15, 15) wall has nucleated, this wall grows at a considerably higher rate than the inner (10, 10) wall. Since both walls advance at comparable rates in the forward direction, this result indicates that the (15, 15) wall grows readily in the reverse direction. Furthermore, since the growth of the (15, 15) wall is quite monotonic, it suggests that no additional nuclei of the (15, 15) wall form before the wall reaches the stationary end of the nanotube. After the third (20, 20) nanotube wall has nucleated, (at the simulation time of 3.2 s), the growth rate of the (10, 10) and (15, 15) nanotube walls decreases to about 5 nm s^{-1}. This nearly 50% additional decrease in the growth rate is consistent with the associated increase in the average number of the edge sites (50 in a (10, 10)+(15, 15) two-wall carbon nanotube vs. 90 in a (10, 10)+(15, 15)+(20, 20) three-wall carbon nanotube). After the fourth (25, 25) nanotube wall has nucleated at the simulation time of ~6.5 s, the growth rate of the (10,

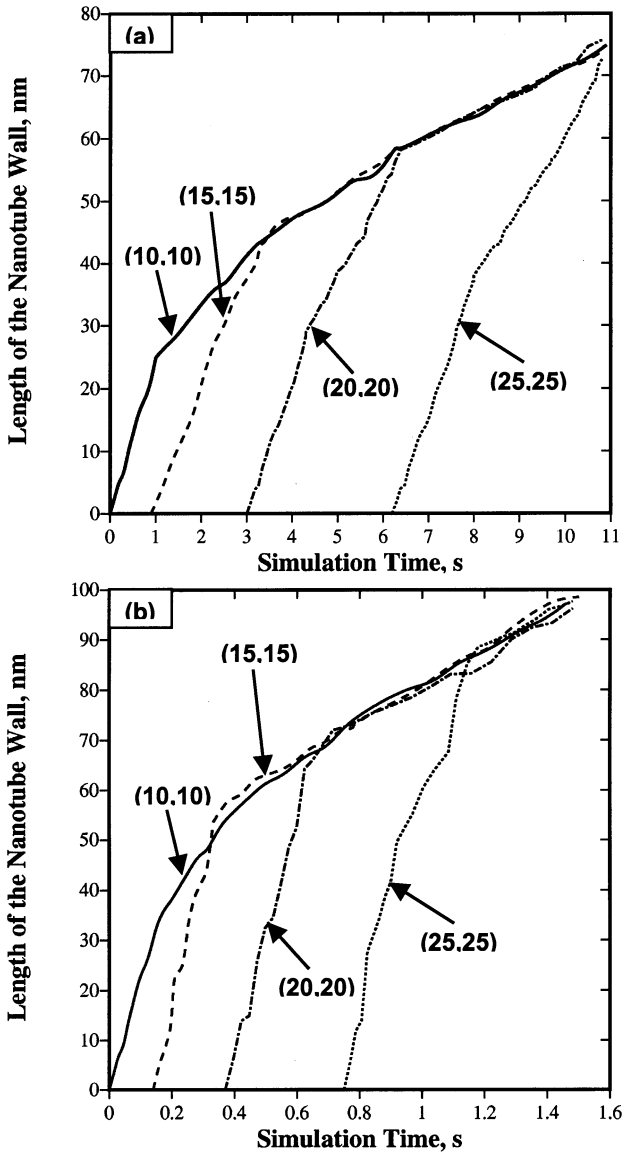

Fig. 5. Temporal evolution of the lengths of the four nanotube walls. The CVD processing conditions correspond to the ones used by: (a) Buckenstein and Hu [26] and (b) Flahaut et al. [27].

10), (15, 15) and (20, 20) nanotube walls decrease to about 3 nm s^{-1}. Again, the nearly 40% additional decrease in the growth rate is consistent with the associated increase in the average number of the edge sites (90 in a (10, 10)+(15, 15)+(20, 20) three-wall carbon nanotube vs. 140 in a (10, 10)+(15, 15)+(20, 20)+(25, 25) four-wall carbon nanotube). Also, as in the case of the (15, 15) wall, the third (20, 20) and the fourth (25, 25) nanotube walls grow at a considerable higher rate in the reverse direction (without apparent formation of additional nuclei) until they reach the stationary end of the interface.

Atomic simulation results under the same (nominal) CVD processing conditions but at the other two axial locations, (the results not shown here for brevity), are found to be qualitatively very similar to the ones shown in Fig. 4(a)–(c). The growth rates at the same simulation times are found to be ~19% lower at a distance 1 in. away from the reactor entrance and ~10% lower at a distance of 1 in. away from the reactor exit relative to the ones shown in Fig. 5(a). These findings are in excellent agreement with their continuum counterparts obtained in our recent reactor-scale analysis of CVD of carbon nanotubes [18].

Temporal evolution of the carbon nanotube morphology during growth under the CVD processing conditions corresponding to those used by Flahaut et al. [27] at the midpoint of the reactor is displayed in Fig. 6(a)–(c). The three configurations displayed in these figures correspond to the simulation times (listed in the caption of Fig. 6(a)–(c)) slightly greater than the ones associated with nucleation of the three non-innermost nanotube walls. A comparison of the results shown in Fig. 6(a)–(c) with the corresponding results shown in Fig. 4(a)–(c) indicates that the nanotube morphology undergoes similar evolution for the two CVD processing conditions. That is, nucleation of the new walls takes place near the growing end of the nanotube and the edge of the nanotube remain rough during the growth process. The major difference between the two sets of results is that the nucleation (as well the growth) rates for the new walls are considerable higher for the CVD processing conditions corresponding to the ones used by Flahaut et al. [27], (please compare the corresponding simulation times in Fig. 4(a)–(c) and Fig. 6(a)–(c)). This finding is consistent with the higher reactor-wall temperature (1343 vs. 1023 K) used by Flahaut et al. [27].

Temporal evolution of the lengths of the four nanotube walls during growth under the CVD processing conditions consistent with the ones used by Flahaut et al. [27] at the midpoint of the reactor are displayed in Fig. 5(b). As in the case of Fig. 5(a), only the (10, 10) wall is present at the beginning of the simulation process and, consequently, its growth rate is quite high (of the order of 220 nm s^{-1}). This growth rate is higher than its counterpart in Fig. 5(a) by about an order of magnitude. Also, as in the case of Fig. 5(a), nucleation of any additional nanotube wall gives rise to a decrease in the (forward) nanotube growth rate by a factor which is approximately equal to the ratio of numbers of the nanotube edge sites after and before nucleation of a new wall. Further similarities between the results displayed in Fig. 5(a) and (b) include high growth rates of newly nucleated walls in the reverse direction until they reach the stationary end of the nanotube. However, the results shown in Fig. 5(b) show occasional surges in the growth rates of new walls in the reverse direction. Careful examination of the nanotube atomistic structure revealed that this behavior is found to be related to the formation of additional nuclei of these walls as the walls advance in the reverse direction. Consequently, when a

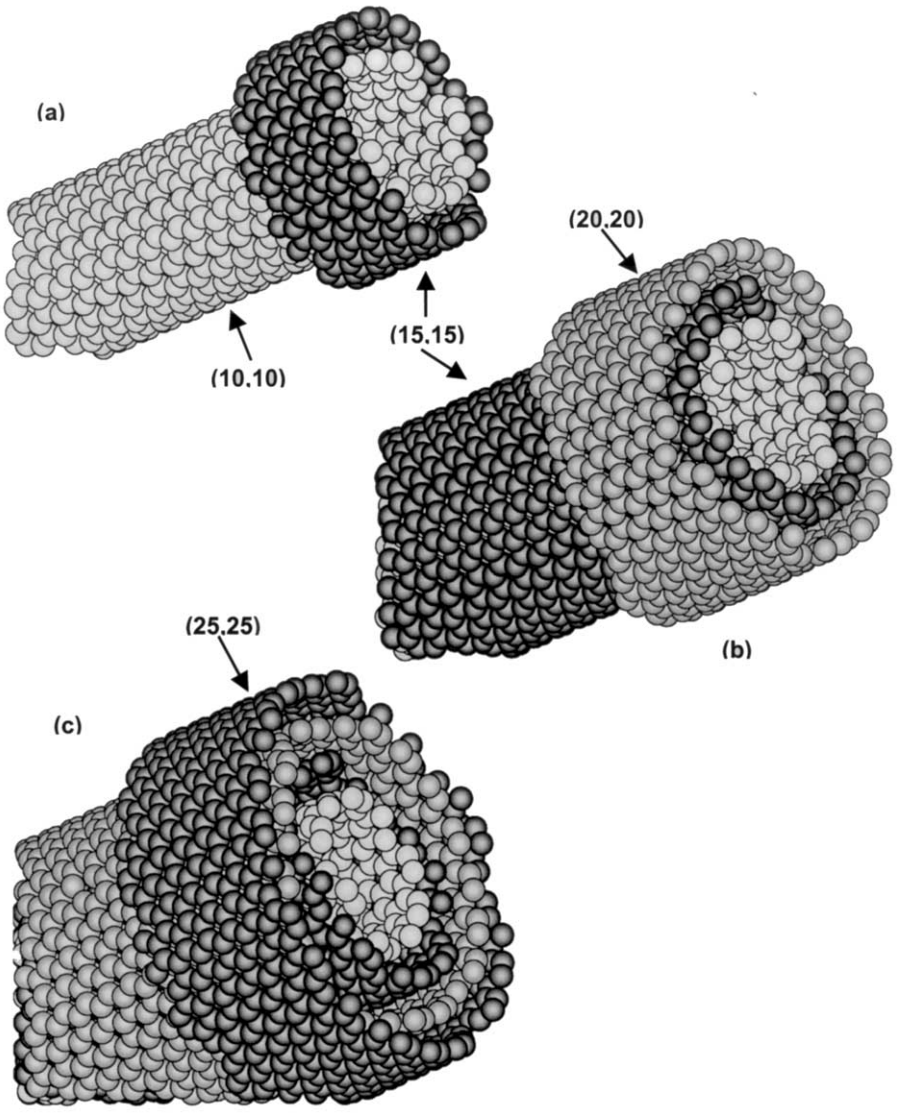

Fig. 6. The nanotube morphology at three different simulation times: (a) 0.15 s; (b) 0.39 s; and (c) 0.77 s. The corresponding total nanotube lengths are 36, 59 and 74 nm, respectively. The CVD processing conditions correspond to the ones used by Flahaut et al. [27].

wall encounters one such nucleus, its length increases instantaneously.

Atomic simulation results corresponding to the nominal CVD processing conditions used by Flahaut et al. [27] but at the other two axial locations, (the results not shown here for brevity), are found to be qualitatively very similar to the ones shown in Fig. 6(a)–(c). The growth rates at the same simulation times are found to be $\sim$12% lower at a distance 1 in. away from the reactor entrance and $\sim$15% lower at a distance of 1 in. away from the reactor exit relative to the ones shown in Fig. 5(a).

The results presented so far indicate that even when formation of a nanotube begins with a transition-metal particle assisted nucleation of a single nanotube wall, additional walls readily nucleate and grow. While the present work is confined to four-wall nanotubes, the results suggest that the fifth, sixth, etc. wall would also form, as long as the transfer of carbon atoms from the transition-metal particle to the nanotube tip and to the nanotube surface can take place. This, in turn, is expected to be the case as long as the radius of the transition-metal particles is larger (or slightly smaller) than that of the outermost wall of the nanotube. Once this condition is not fulfilled any longer, formation of new walls relies solely on the reactions occurring at the surface of the outermost nanotube wall and, consequently, could take place at a considerably lower rate. In other words, the results obtained in the present work suggest that the final diameter of a nanotube should be very close to that of the transition-metal particle attached to its tip. This prediction is consistent with a number of experimental observations e.g. [9].

The results presented in the present work further indicate that nanotube growth rates are not only higher at higher temperatures, but that the existing nanotube walls also grow to a larger length before a new wall is nucleated. This finding seems to suggest that at sufficiently high temperatures one may, perhaps, produce SWCNTs. To test this hypothesis, atomic scale simulations are carried out at the reactor-wall temperature of 1800 K. The results obtained show that while nucleation of the second wall is significantly delayed and the SWCNT could grow to a length of approximately ~ 160 nm before the second wall is nucleated. However, as shown in Fig. 7, the as-grown SWCNTs generally contain numerous defects (atoms missing from their regular positions). To improve clarity of the lattice defects, they are denoted as small dark spheres in Fig. 7. Unless the observed defects can be eliminated by subsequent annealing, they could seriously degrade the properties of the SWCNTs. Since the present model does not account for diffusion of lattice defects within the nanotube walls, this phenomenon will be incorporated in the kinetic Monte Carlo analysis of the fabrication of carbon nanotubes by CVD in our future work.

4. Conclusions

Based on the results obtained in the present work, the following main conclusions can be drawn:

(1) Due to a relative ease with which new nanotube walls can form and grow, the fabrication of SWCNTs by transition-metal particles catalytically-assisted thermal decomposition of methane appears to be a formidable task.

(2) While higher reactor-wall temperatures favor the growth of nanotubes relative to the nucleation of new walls and are hence beneficial from the standpoint of producing SWCNTs, they also promote formation of lattice defects which could seriously compromise the performance of carbon nanotubes.

(3) Kinetic Monte Carlo simulations of the fabrication of carbon nanotubes by transition-metal particle catalytically-assisted thermal decomposition of methane appear to be a powerful tool which can successfully predict a number of experimentally observed phenomena (e.g. the nanotube diameter is closely related to that of the transition-metal particle attached to its tip, the effect of nominal and local processing conditions on the growth rates of carbon nanotubes, etc.).

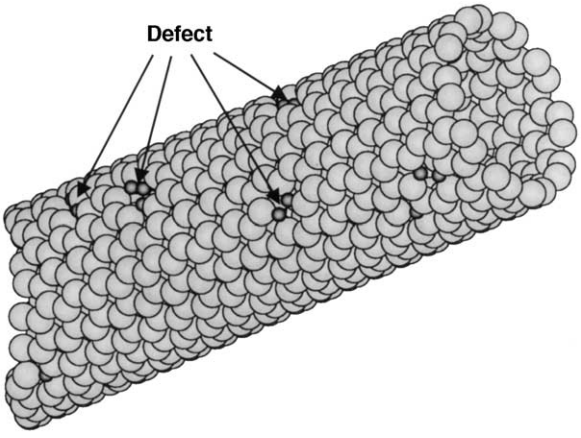

Fig. 7. The morphology of a nanotube grown at 1800 K. Missing carbon atoms are denoted using small dark spheres.

Acknowledgements

The material presented in this paper is based on work supported by the US Army Grant Number DAAD19-01-1-0661. The authors are indebted to Drs Walter Roy, Fred Stenton and William DeRosset of ARL for the support and a continuing interest in the present work. The authors also acknowledge the support of the Office of High Performance Computing Facilities at Clemson University.

Appendix A: Kinetic Monte Carlo time increment

In this section a rigorous proof is provided for the variable time increment Δt defined by Eq. (7). Toward that end, it is useful to consider a system which involves in time as various events take place. In conventional kinetic Monte Carlo simulations, a constant time increment is used such that at most one event occurs during each time increment. This is shown schematically in Fig. 8(a). This approach is useful for studying the evolution of systems that can evolve through an infinite number of distinct events. However, if the number of events by which the system can evolve is finite and enumerable, then a more efficient approach can be

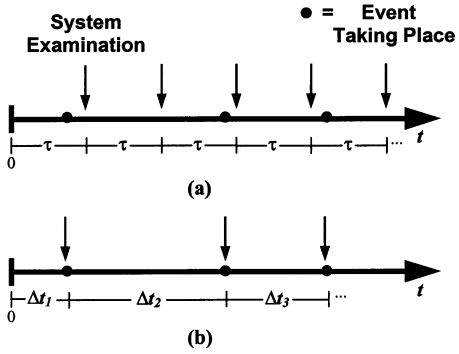

Fig. 8. Schematics of temporal sampling schemes in: (a) the conventional kinetic Monte Carlo at fixed time intervals and (b) the present Monte Carlo methods at dynamically adopted time intervals. Vertical arrows are used to denote time intervals at which the system is examined while filled circles are used to denote events occurrences.

adopted. Instead of examining the system at fixed time intervals, and determining which events occur and when, the system can be examined only when an event occurs, and the time increment itself can be calculated at each step. This is shown schematically in Fig. 8(b). This technique is particularly useful in situations where the events occur on very different time scales and the fastest events (which entail smallest time increments) are only possible in certain rate system configurations.

In the present kinetic Monte Carlo scheme shown schematically in Fig. 8(b), the time increment that has elapsed since the last event has to be determined at each simulation step. This is done by applying the following procedure: first, the probability that an event will occur during some infinitesimal time interval, dt, is defined as Πdt, where Π is the average number of all possible events that occur per unit time. Hence, the probability that no event occurs during time dt is $(1-\Pi dt)$. If the time at which the most recent event occurred is set as $t=0$, and the probability that no event occurs in time Δt since the last event is denoted $P(\Delta t)$. Then the probability that no event occurs during time $\Delta t+dt$, $P(\Delta t+dt)$, is equal to the product of the probability that no event occurs during the time interval Δt and the one that no event occurs during the additional time increment dt, i.e.:

$$P(\Delta t + dt) = P(\Delta t)(1-\Pi dt) \tag{A.1}$$

Eq. (A.1) can be rewritten as a differential equation,

$$\frac{dP(\Delta t)}{dt} = -P(\Delta t)\Pi \tag{A.2}$$

which has the solution:

$$P(\Delta t) = \exp(-\Pi \Delta t) \tag{A.3}$$

since $P(0)=1$. Following the Metropolis Monte Carlo procedure in which configurational transitions which increase the system energy are either accepted or rejected based on a comparison between a Boltzman distribution based transitional probability and a random number, $P(\Delta t)$ is assigned a random number, ξ_2, evenly distributed in the range (0, 1) in Eq. (A.3). If Eq. (A.3) is then solved for Δt one obtains the relation:

$$\Delta t = -\frac{\ln(\xi_2)}{\Pi} \tag{A.4}$$

which can be compared directly with Eq. (7).

References

[1] S. Iijima, Nature 354 (1991) 56.
[2] M.M.J. Treacy, T.W. Ebbesen, J.M. Gibson, Nature 381 (1996) 678.
[3] H. Dai, J.H. Hafner, A.G. Rinzler, D.T. Cebert, R.E. Smalley, Nature 384 (1996) 147.
[4] A.C. Dillon, K.M. Jones, T.A. Bekkedahl, C.H. Kiang, D.S. Bethune, M.J. Heben, Nature 386 (1997) 377.
[5] M.S. Dresselhaus, G. Dresselhaus, P.C. Eklund, Science of Fullerens and Carbon Nanotubules, Academic Press, San Diego 1996.
[6] S.J. Tans, R.M. Verschueren, C. Dekker, Nature 393 (1999) 40.
[7] A. Thess, R. Lee, P. Nikolaev, H. Dai, P. Petit, J. Robert, C. Xu, Y. Lee, S. Kim, A.G. Rinzler, D.T. Colbet, G.E. Scuseria, D. Tomanek, J.E. Fischer, R.E. Smalley, Science 273 (1996) 483.
[8] P. Kim, C.M. Lieber, Science 285 (1999) 2140.
[9] R. Andrews, D. Jacques, A.M. Rao, F. Derbyshire, D. Qian, X. Fan, E.C. Dickey, J. Chen, Chem. Phys. Lett. 303 (1999) 467.
[10] M. Terrones, N. Grobert, J. Olivares, J.P. Zhang, H. Terrones, K. Kordatos, W.K. Hsu, J.P. Hare, P.D. Townsend, K. Prassides, A.K. Cheetham, H.W. Kroto, D.R.M. Walton, Nature 388 (1997) 52.
[11] J. Li, C. Papadopoulos, J.M. Xu, M. Mciskovits, Appl. Phys. Lett. 75 (1999) 367.
[12] A. Maitin, C.J. Brabec, C. Roland, J. Bernholc, Phys. Rev. 52 (1995) 14850.
[13] Y.H. Lee, S.G. Kim, D. Tomanek, Phys. Rev. Lett. 24 (1997) 2393.
[14] J.-C. Charlier, A.D. Vita, X. Blasé, R. Car, Science 275 (1997) 646.
[15] M. Grujicic, S.G. Lai, J. Mater. Sci. 35 (2000) 5359.
[16] M. Grujicic, S.G. Lai, J. Mater. Sci. 35 (2000) 5371.
[17] M. Grujicic, S.G. Lai, J. Mater. Synthesis and Processing 8 (2000) 73.
[18] M. Grujicic, G. Cao, B. Gersten, J. Mater. Sci., submitted for publication.
[19] M. Grujicic, G. Cao, B. Gersten, Appl. Surf. Phys., submitted for publication.
[20] SURFACE CHEMKIN III User Manual, Sandia National Laboratories, San Diego, CA, 1996.
[21] C.J. Lee, S. Kim, D. Tomanek, Appl. Phys. Lett. 75 (1999) 1721.
[22] C.C. Battaile, D.J. Srolovitz, J.E. Butler, J. Appl. Phys. 82 (1997) 6293.
[23] R.T.K. Baker, P.S. Harris, Formation of Filamentous Carbon in Chemistry and Physics of Carbon 14, Marcel Dekker, New York 1978, p. 83.
[24] N. Kittamura, A. Oshiyama, J. Physical Soc. Jpn. 70 (2001) 1995.
[25] D.E. Goldberg, Genetic Algorithms in Search, Optimization and Machine Learning, Addison-Wesley, Reading, MA 1989.
[26] E. Buckenstein, Y.H. Hu, Carbon 36 (1998) 275.
[27] E. Flahaut, A. Govindaraj, A. Peigney, Ch. Laurent, A. Rousset, C.N.R. Rao, Chem. Phys. Lett. 300 (1999) 236.
[28] G. Cao, PhD Thesis in Progress, Clemson University, November 2001.